Article

Energy and Information Fluxes at Upper Ocean Density Fronts

Pablo Cornejo [1,‡], Adolfo Bahamondes [2,‡]

[1] Department of Mechanical Engineering, Faculty of Engineering, University of Concepción, Concepción, Chile; pabcornejo@udec.cl
[2] Department of Geophysics, Faculty of Physical and Mathematical Sciences, University of Concepción, Concepción, Chile; adbahamonde@udec.cl
* Correspondence: pabcornejo@udec.cl; Tel.: +56 41 2203547
† Interdisciplinary Center for the Aquaculture Research (INCAR),Concepción,Chile

Abstract: We present large eddy simulations of a mid-latitude open ocean front using a modified state of the art computational fluid dynamics code. We investigate the energy and information fluxes at the submesoscale/small-scale range in the absence of any atmospheric forcing. We find submesoscale conditions ($Ro \sim 1$, $Ri \sim 1$) near surface, within baroclinic structures related with partially imbalanced frontogenetic activity. Near surface, the simulations show a significant scale coupling on scales larger than $\sim 10^3$ (m). This is manifested as a strong direct energy cascade and intense mutual communication between scales, where the latter was evaluated using an estimator based on Mutual Information Theory. At scales smaller than $\sim 10^3$ (m) the results show near-zero energy flux, however, at this scale range, the estimator of mutual communication still shows values corresponding with a significant level of communication between them. This fact motivates to investigate the nature of the self-organized turbulent motion at this scale range with weak energetic coupling but where communication between scales is still significant and to inquire into the existence of synchronization or functional relationships between scales with emphasis on eventual underlying non-local processes.

Keywords: Submesoscale; Turbulence; Frontogenesis; Energy cascade; Mutual communication; Ocean density fronts

1. Introduction

In the last two decades numerical predictions and observations have revealed a richness of turbulent submesocale processes in the upper ocean. Within these interesting turbulent upper ocean processes, there has been special interest in the study of density fronts due to the motivation of strengthening the understanding of the processes that catalyze smaller-scale motion in order to understand and parameterize them. Such processes include frontogenesis [1,2], frontal instabilities and breakdown of balanced flow [3–6] and their role in promoting the collapse of baroclinical waves and the generation of submesoscale eddies, the mixed-layer restratification [7], the flattening of the spectra in the submesoscale range [8], the develop of direct energy cascade [9,10] and the development of high vertical velocities [4,6,11], as well as their important implications for primary productivity and climate [11].

Density fronts are ubiquitous in the ocean. They tilt the isopycnals and hence restratifies the mixed layer and cause a secondary circulation with high vertical velocities [12,13]. The main departure from balance occurs in the vicinity of fronts where the flow is strongly affected by the secondary circulation which involves frontogenesis [8] and which can also be promoted by alongfront winds [14]. Fronts have also been identified as regions with high energy dissipation, high turbulent mixing [2] and where the direct energy cascade can take place given the high vertical shear due to frontogenesis [15].

Recent research on complex systems and turbulence have investigated the characteristics of communication [16–18] and information flows [19,20] between the scales of

 doi:10.20944/preprints202211.0347.v1

motion, giving an alternative standpoint that allows building a more complex picture of the phenomenon of turbulence by complementing the current purely dynamic view based on classical mechanics with features from information theory.

The aim of the present manuscript is to investigate the energy and information fluxes at the submesoscale/small-scale range in a mid-latitude upper ocean front using results from a highly resolved LES model allowing to simulate the submesoscale – small scale range directly in order to analyze the characteristics of information flow in the context of current knowledge of this widely studied turbulent system. A state-of-the-art Computational Fluid Dynamics (CFD) code is used to adapt a Large Eddy Simulation (LES) model for geophysical flows. This configuration and the detailed description of hydrodynamics and turbulence modeling was previously reported by [21].

2. Computational Model

Simulations were performed using a periodic, non-hydrostatic LES model [21]. The state of the art CFD code ANSYS-FLUENT was modified to include Earth's rotation and water column stratification in order to describe geophysical fluid flows. For the calculation of subgrid stresses, the well known Smagorinsky model [22] is modified to employ a non-isotropic computational grid introducing the correction proposed by [23] in the calculation of the mixing length. This modification allows us to use non-isotropic grids when the usage of an isotropic grid is prohibitive due to limitations regarding computational capacity. The model domain has the size of 10 km in the crossfront direction, 5 km in the alongfront direction, and 500 m depth (Fig.1.a). The domain is discretized with 2.2×10^6 cells, with a hexahedral grid of 24 m for the horizontal resolution, a constant 3 m vertical resolution within the first 50 m depth, a stretched vertical resolution between 50 m (dz = 3 m) – 250 m (dz = 24 m) depth and a constant 24 m vertical resolution between 250 m – 500 m depth. The model time step is 120 s.

The domain alongfront direction is periodic, and the crossfront direction as well as the top and bottom are taken to be stress free boundaries. We use Second Order Discretization Schemes and the Least Squares Cell Based Method for calculating the gradients. For the pressure-velocity coupling the SIMPLE (semi-implicit method for pressure-linked equations) algorithm is adopted.

The model is initialized with a 50 m depth mixed layer and stable stratification between 50 m and 500 m. Within the first 50 m depth the density distribution in the crossfront direction is given by

$$\rho(y,0) = \frac{1}{2}\Delta\rho\frac{(1-exp(\frac{y}{2}))}{(1+exp(\frac{y}{2}))} \tag{1}$$

with $\Delta\rho = 0.1\ kg/m^3$, where y represents the horizontal coordinate in the acrossfront direction, Fig.1.b. Below the mixed layer, horizontal density gradient extends up to a depth of 250 m. In this zone

$$\Delta\rho = 0.1\frac{(250+z)}{200} \tag{2}$$

where z is the vertical coordinate. The velocity field is initialized with a baroclinic jet in thermal wind balance

$$u = -\frac{1}{\rho f}\frac{\partial p}{\partial y} \tag{3}$$

where u is the velocity in the alongfront direction and the pressure p is estimated from the hydrostatic balance

$$\frac{\partial p}{\partial z} = -\rho g \tag{4}$$

Preprints (www.preprints.org) | NOT PEER-REVIEWED | Posted: 18 November 2022 doi:10.20944/preprints202211.0347.v1

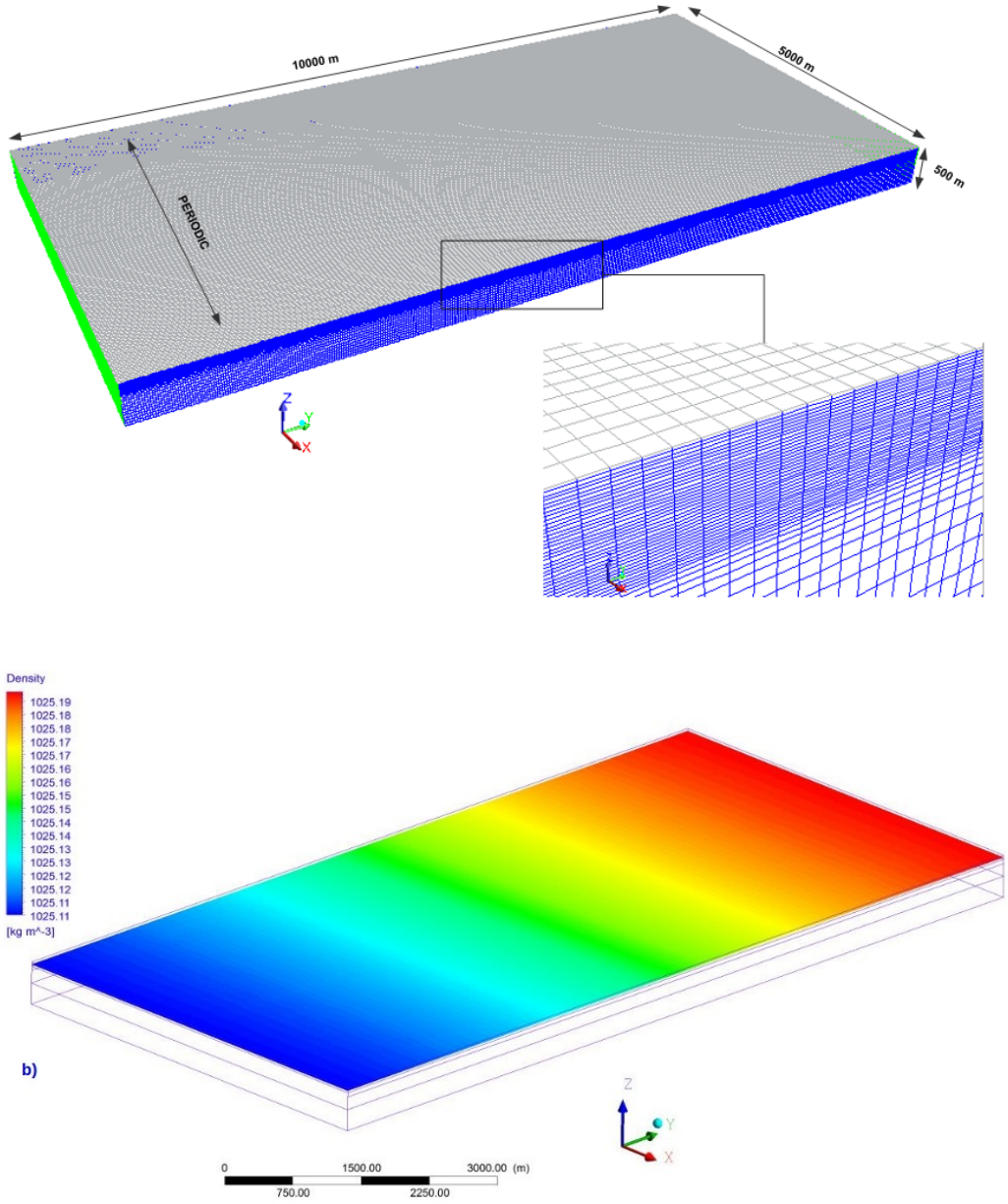

Figure 1. Computational model. Grid and dimensions (top), initial density distribution (bottom).

with g as the acceleration due to gravity. The model was set up using a mid-latitude Coriolis parameter $f = 0.86 \times 10^{-4}\ s^{-1}$. This simulation does not consider any atmospheric forcing (winds, heating, cooling, etc).

Under these conditions Stone's fastest-growing rate length scale and growth time [24,25] reach 3 km and 1 day, and both are well resolved with the domain size, grid resolution and time step.

3. Energy transfer, hydrodynamics, and information processes

3.1. Energy transfer and hydrodynamics processes

A spectral representation of kinetic energy balance is presented below (Equation 5), where the local variation of kinetic energy in the wave number space is estimated by the sum of the right-side terms which describe from left to right the advection of kinetic energy, pressure work, the buoyancy term and dissipation.

Preprints (www.preprints.org) | NOT PEER-REVIEWED | Posted: 18 November 2022 doi:10.20944/preprints202211.0347.v1

$$\frac{1}{2}\frac{\partial \widehat{u}\cdot\widehat{u}^*}{\partial t} = -\widehat{u}\cdot\left(\widehat{u\cdot\nabla}\right)u^* + \widehat{u}\cdot\widehat{\nabla p}^* + \widehat{w}\cdot\widehat{b}^* + \widehat{u}\cdot\widehat{D}^* \tag{5}$$

Here u is the velocity vector, p the pressure, w denotes vertical velocity component, b the buoyancy and D the dissipative term. The operators $\widehat{(\cdot)}$ and $(\cdot)^*$ denote the Fourier transform and conjugate respectively. Through the integration of advective term of Eq.5 over an appropriate k shell $[k = 0$ to $k_h]$, it is possible to estimate the spectral kinetic energy flux and express the kinetic energy cascade explicitly as,

$$\Pi(k) = -\int_{k=0}^{k=k_h} \widehat{u}\cdot\left(\widehat{u\cdot\nabla}\right)u^* dk \tag{6}$$

where k_h the maximum wavelength allowed by domain dimensions.

The intensity of frontogenesis can be addressed by the calculation of the frontogenesis parameter (F_s) which is a measure of the modification of the horizontal buoyancy gradient magnitude due to the straining by the geostrophic flow [6,8,13] where,

$$F_s = Q_s \cdot \nabla_h \rho \tag{7}$$

$\nabla_h\rho$ is the horizontal density gradient, and the Q vector is given by

$$Q_s = -\left(\frac{\partial u}{\partial x}\frac{\partial \rho}{\partial x} + \frac{\partial v}{\partial x}\frac{\partial \rho}{\partial y}, \frac{\partial u}{\partial y}\frac{\partial \rho}{\partial x} + \frac{\partial v}{\partial y}\frac{\partial \rho}{\partial y}\right) \tag{8}$$

Here u, v are the horizontal velocity components in the x, y directions and ρ the density.

Given We are interested in determining if the processes promoting the direct energy cascade are related to a balanced or unbalanced dynamics. The balance of pressure, Coriolis and centrifugal forces are expressed as in [26],

$$-\nabla_h\cdot(u_h\cdot\nabla_h u_h) + f\zeta^z - \frac{1}{\rho}\nabla_h^2 p = 0 \tag{9}$$

The degree of imbalance is assessed by the normalized error in the gradient wind balance

$$\epsilon_{gw} = \frac{|-\nabla_h\cdot(u_h\cdot\nabla_h u_h) + f\zeta^z - \frac{1}{\rho}\nabla_h^2 p|}{|\nabla_h\cdot(u_h\cdot\nabla_h u_h)| + f|\zeta^z| - |\frac{1}{\rho}\nabla_h^2 p| + \mu} \tag{10}$$

Here,

$$\mu = f\zeta^z_{RMS} + |\frac{1}{\rho}\nabla_h^2 p|_{RMS} \tag{11}$$

is added to avoid the appearance of strong imbalance in regions of the flow where circulation is weak [8,27]. The magnitude of ϵ_{gw} near 0 indicates balanced dynamics, whereas values near 1 indicate the presence of fully unbalanced processes.

3.2. Information related processes

Shannon's entropy is a quantity associated with the information content in a complex system, interpreted in a statistical sense. If the probability of an event is 1, then it does not give us information, we know that the event will always happen. The same thing happens when the probability is 0, we don't get information about those events since they never happen. Due to these properties, entropy is a concave functional in the probability density function: it reaches a maximum between probability 0 and 1. Therefore, entropy can be interpreted as the information content or predictability of a system: the higher the entropy, the less predictable the system. On the other hand, mutual information measures the amount of information shared between two systems, this can be interpreted as the information contained in the correlations or interactions of two systems: If the systems are independent then the mutual information is zero and their joint probability can be broken

Preprints (www.preprints.org) | NOT PEER-REVIEWED | Posted: 18 November 2022 doi:10.20944/preprints202211.0347.v1

down as a product. Note how mutual information and entropy complement each other: if the mutual information between two systems is zero, then the (joint) entropy of both is simply the sum of their individual entropy, while when they interact there is a contribution to the entropy that is only due to interactions.

If we have a system with a (marginal) probability density $\rho(X)$ and another with a density $\rho(Y)$, their joint density will be $\rho(X,Y)$. The entropy of a single system is defined by,

$$S(x) = \int \rho(X)\log(\rho(X))dX \tag{12}$$

while their mutual information is

$$I(X,Y) = \int\int \rho(X,Y)\log\left(\frac{\rho(X,Y)}{\rho(X)\rho(Y)}\right)dXdY \tag{13}$$

The relationship between both quantities can be summarized in a diagram shown in the Fig-2

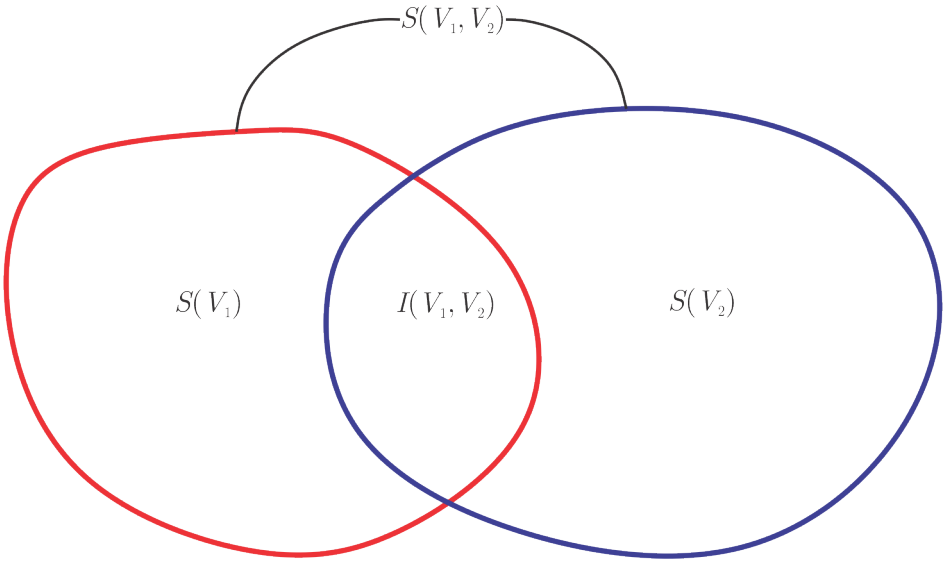

Figure 2. Relationship between entropy and mutual information

One of the problems we face in calculating these quantities is that they depend on density functions, this complicates things especially when they have long probability tails, as in the case of turbulence. Due to this the theory propose the use of estimators, one of the best known and applied are the 'nearest neighbors' type, which we use in this study to calculate entropy and mutual information.

In this work we use the Kozachenko-Leonenko estimator for the entropy [28],

$$S = \psi(N) - \psi(k) + \log c_d + \frac{d}{N}\sum \log(\epsilon_i) \tag{14}$$

In the case of mutual information we use the Kraskov-Stögbauer-Grassberger estimator (KSG) [29]

$$I(X,Y) \approx \psi(N) + \psi(k) - \langle \psi(n_x+1) + \psi(n_y+1)\rangle \tag{15}$$

In both equations $\psi(x)$ represents the digamma function, N the number of data, ϵ_i is a distance dependent on the value of k, (n_x, n_y) are the number of points that are less than ϵ_i apart and $\langle\cdot\rangle$ represents the average. In both estimators we have a free parameter k which is the number of *nearest neighbors* to consider. This is used to determine the value of n_x and n_y in the KSG algorithm and ϵ_i in the KL algorithm. In this study, $k = 4$ is set for the estimation of both quantities (recommended value in previous studies for turbulent systems [17]). The algorithm used for mutual information is the one first proposed by

Preprints (www.preprints.org) | NOT PEER-REVIEWED | Posted: 18 November 2022 doi:10.20944/preprints202211.0347.v1

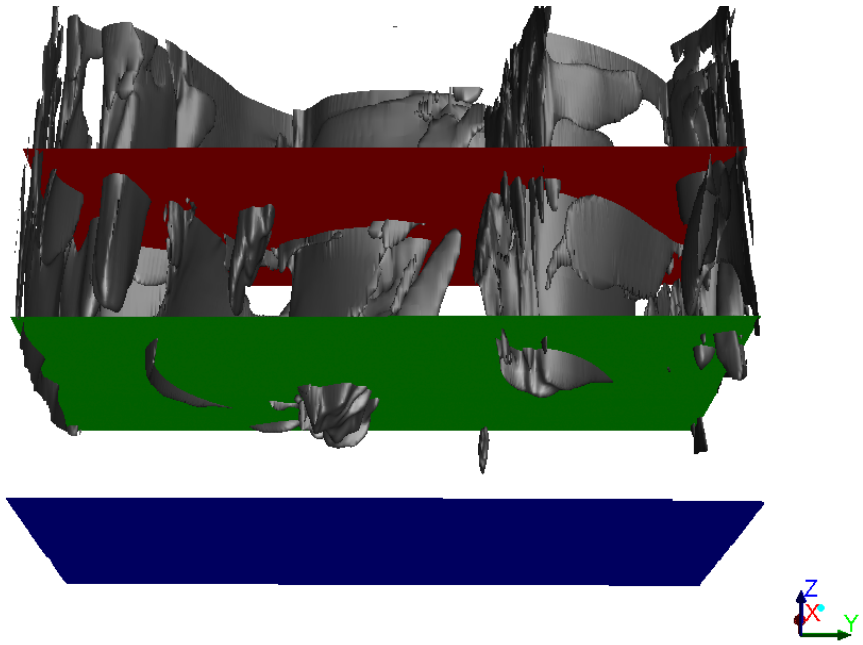

Figure 3. Submesoscale structures ($Ro = 1$ iso-surface) within the mixed layer. Planes at 25 m (red), 50 m (green) and 75 m (blue) depth.

[30], which partitions the $X - Y$ space into a square grid. Finally mention that the distance selected to apply the estimators is the Euclidean distance.

4. Simulation

Using the model described above we simulated the time evolution of the density front for 20 days. The front begins meandering and developing instabilities within the mixed layer two days after initialization. These instabilities become increasingly large in amplitude, resulting in its collapse and subsequent emergence of coherent structures around the fourth day of simulation. Near the seventh day from model initialization turbulence is fully developed. We show results nine days after the model initialization. Results show a strongly unstable shear flow within the first 50 m depth. In Fig.3 we plotted an iso-surface of $Ro = \frac{\zeta}{f} = 1$, the plane colored green is located at 50 m depth. This 3D representation of the submesoscale structures has been overlaid in all snapshots considered in the present analysis, thus one can directly observe the spatial correlation between the variable under consideration and submesoscale structure. Fig.4 shows the velocity field. In contrast to the flow characteristics found within the mixed layer, below 50 m depth the flow is marginally unstable, thereby indicating that even in the unforced case considered here, ocean fronts promote turbulent mixing in the upper ocean, which is consistent with observations [14]. Rossby number distribution were estimated from vertical relative vorticity through $Ro = \frac{\zeta^z}{f}$. Regions of $Ro \sim 1$ were found only in the first 50 m depth within the mixed layer. Inside submesoscale structures the Rossby number takes even higher values as shown in the left panel of Fig.5. At 75 m depth there are only few regions where Rossby number reaches a maximum value of $Ro \sim 0.4$ and $Ro \sim 0.1$ is found in deeper waters at 300 m depth (right panel of Fig.5). Through the inspection of kinetic energy spectra one can indirectly infer some characteristics of the kinetic energy cascade of turbulent flows. The interior quasi-geostrophic theory [31] predicts for the balanced mesoscale flow a kinetic energy spectrum slope of -3 indicating an inverse energy cascade. Submesoscale dynamics has shown to flat the spectral kinetic energy distribution to a -2 slope [4] and although the surface quasi-geostrophic theory [32] predicts the same spectrum's shape, this theory as a model for submesoscale dynamics poorly describes the

Preprints (www.preprints.org) | NOT PEER-REVIEWED | Posted: 18 November 2022 doi:10.20944/preprints202211.0347.v1

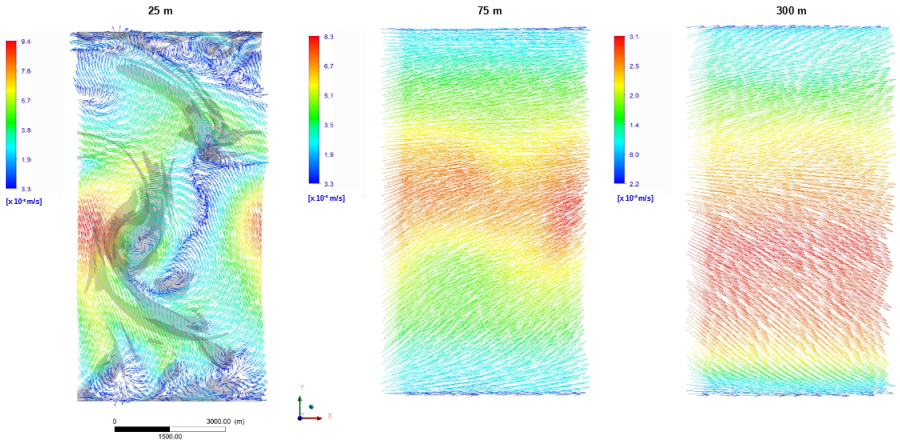

Figure 4. Velocity field, at 25 m depth (left), 75 m depth (middle) and 300 m depth (right). The structures in grey are the projections of $Ro = 1$ iso-surface.

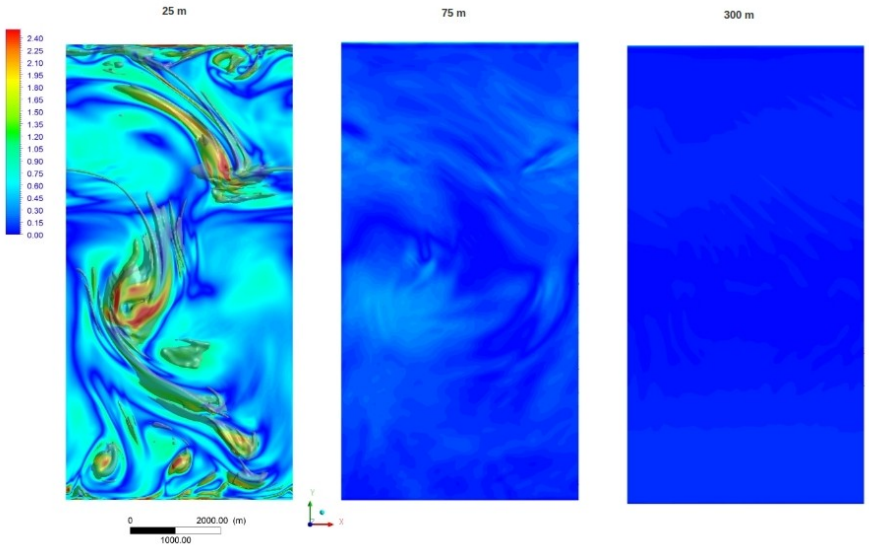

Figure 5. Rossby number distribution, at 25 m depth (left), 75 m depth (middle) and 300 m depth (right).

direct kinetic energy cascade present in simulations including non-geostrophic processes [33]. In this case the surface quasigeostrophic theory including non-gestrophic processes predicts a spectrum with a slope of -5/3 [34]. We computed 1D kinetic and potential energy spectra using transects of horizontal velocity and density variation at different depths, Fig.6. Turbulent structures are found to be more energetic within the top 50 m mixed layer. In this region the spectrum is flatter than the spectrum computed at 75 m depth in the range of length scale between [0 m -125 m] which is in agreement with previous work [4,11]. The calculations of the spectral kinetic energy flux plotted in Fig.7 indicate that in the near ocean surface region at 25 m depth, a strong direct kinetic energy flux occurs for the horizontal scales larger than 1 km. At the same depth, for scales somewhat smaller than 1 km, results show an inverse kinetic energy flux of similar magnitude to the inverse kinetic energy flux that takes place a 75 m depth for horizontal scales larger 2.5 km. In deeper waters the spectral kinetic energy flux is weak.

Preprints (www.preprints.org) | NOT PEER-REVIEWED | Posted: 18 November 2022 doi:10.20944/preprints202211.0347.v1

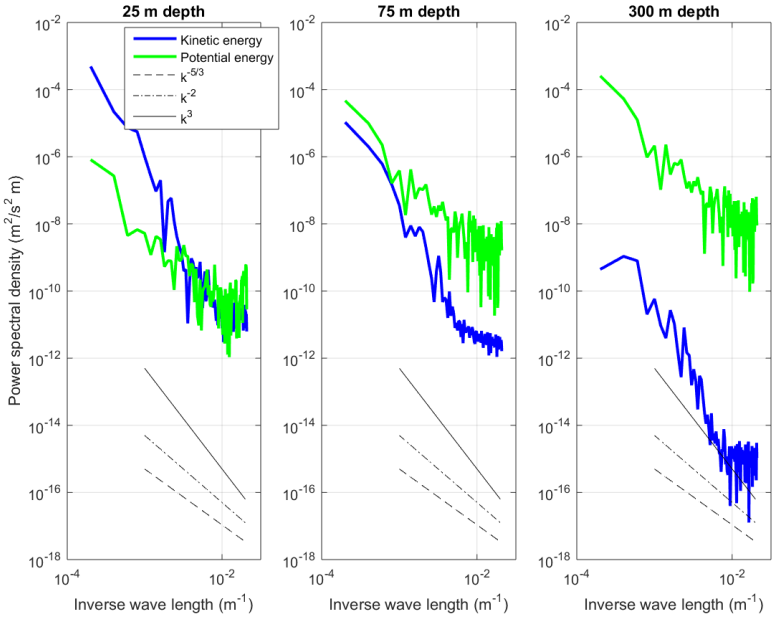

Figure 6. Along the front 1-D kinetic energy and available potential energy wave number spectra.

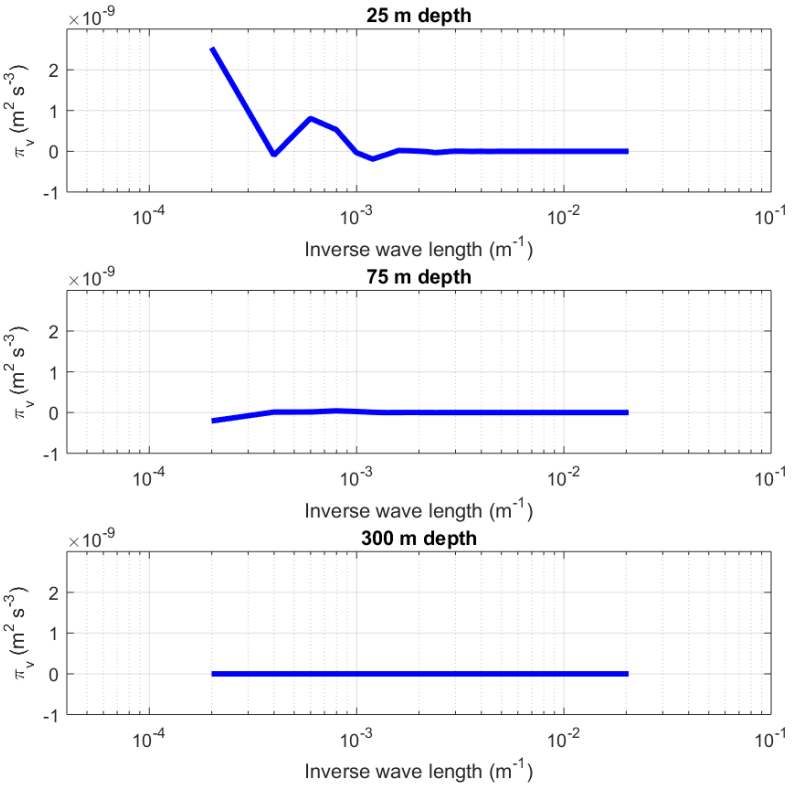

Figure 7. Kinetic energy flux

Preprints (www.preprints.org) | NOT PEER-REVIEWED | Posted: 18 November 2022 doi:10.20944/preprints202211.0347.v1

In LES models subgrid momentum diffusion is also a measure of the turbulent kinetic energy dissipation at the subgrid scale [35]. Fig.8 shows the subgrid momentum diffusion at 25 m, 75 m and 300 m depth. Near surface results show large zones of high subgrid momentum diffusion while at higher depths these zones become smaller in extension and intensity. These findings are not surprising and go in the same direction as the predictions of the direct kinetic energy flux: in the absence of atmospheric forcing and due to frontal processes the upper ocean is subject of direct kinetic energy flux and high subgrid momentum diffusion.

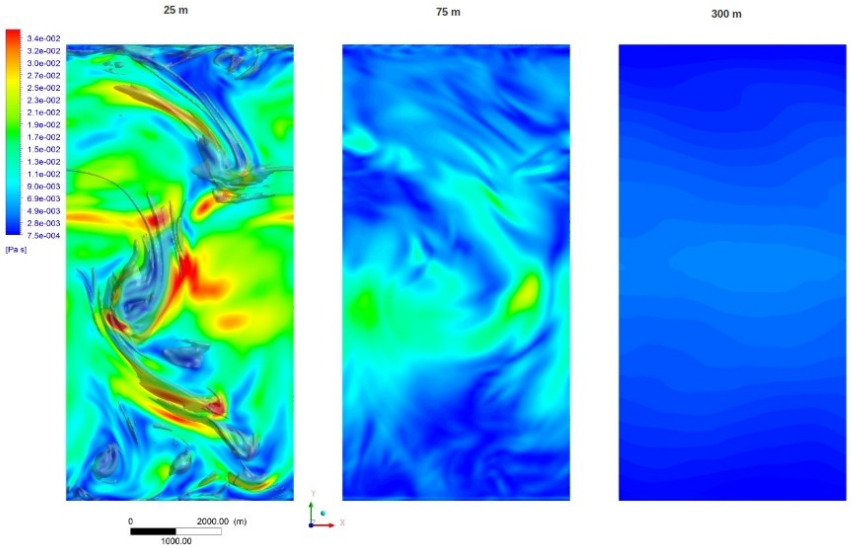

Figure 8. Subgrid momentum diffusion distribution, at 25 m depth (left), 75 m depth (middle) and 300 m depth (right).The $Ro = 1$ iso-surface projection is showed as a grey region.

Difference from the gradient wind balance is computed and plotted in Fig.10. In agreement with [8], the unbalanced pattern is found to be affected by the frontogenetic activity (Fig.**??**). Processes within the mixed layer are found to be partially imbalanced, where only a few small regions adjacent to the submesoscale structures reach values near 0.8. However, apart from these limited small regions ϵ_{gw} reaches values between $0.4 \sim 0.6$ and this way it is not possible to assess the predominance of balanced or unbalanced processes in the promotion of the direct kinetic energy flux.

Given turbulence is a scaling phenomenon we study the entropy distribution in Fourier space. We use the same 1D velocity transects employed to calculate kinetic energy fluxes to perform entropy calculations. The velocity field is filtered according to

$$u_{k<} = \int_{q \leq k} u_q e^{iqx} dq \qquad u_{k>} = \int_{q \geq k} u_q e^{iqx} dq \tag{16}$$

Therefore we can decompose the velocity field into two parts $u = u_{k<} + u_{k>}$ associated with the large scale ($u = u_{k<}$) and the small scale ($u = u_{k>}$), and where both range interact: the evolution of the small scale is not independent of the large scale. Therefore to complement the entropy we calculate the mutual information between both parts $I(u_{k<}, u_{k>})$.

Results for entropy are shown in Fig.11. We observe a decrease in the entropy for the small scales (black line), while for large scales entropy quickly saturates (red line).

In Fig.12 is shown the mutual information between the filtered velocity fields. The apparent sharp increase in mutual information near the maximum wave number is probably due to the fact that we are approaching the minimum resolution of the simulation, so that part of the results should not be considered as reliable.

Preprints (www.preprints.org) | NOT PEER-REVIEWED | Posted: 18 November 2022 doi:10.20944/preprints202211.0347.v1

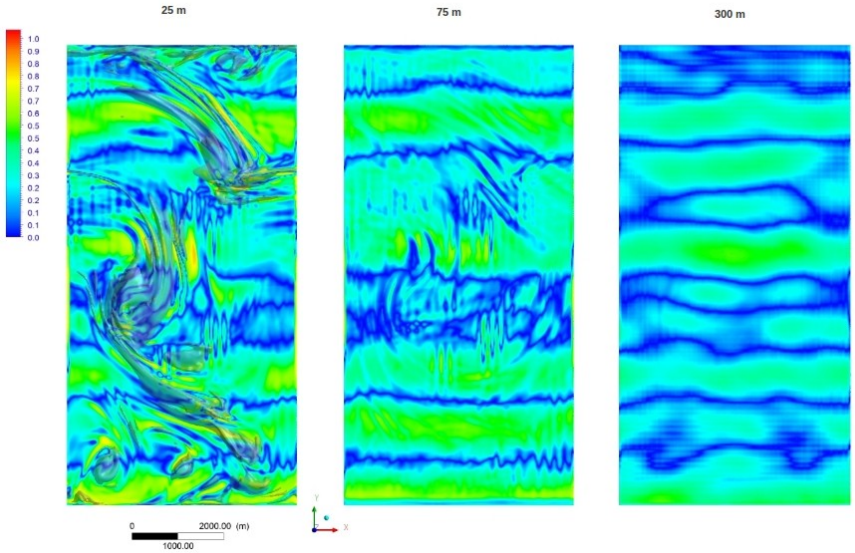

Figure 9. Error in the wind gradient balance, at 25 m depth (left), 75 m depth (middle) and 300 m depth (right). The $Ro = 1$ iso-surface projection is showed as a grey region.

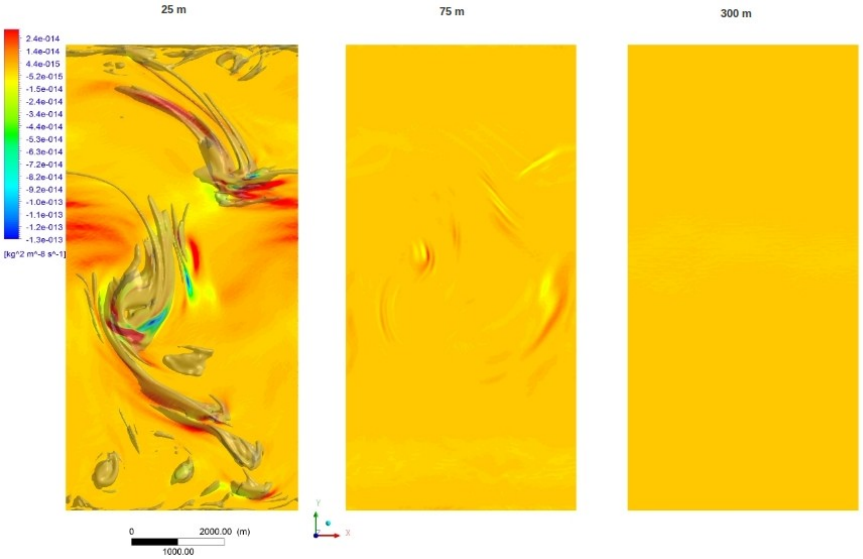

Figure 10. Frontogenesis factor, at 25 m depth (left), 75 m depth (middle) and 300 m depth (right). The $Ro = 1$ iso-surface projection is showed as a grey region.

We observe a logarithmic decrease in entropy (note that the scale of the k axis is logarithmic), this behavior has been observed before in the inertial range ([**?**]). In this case we observe that the decrease in information is characterized by a slope of approx. -1.4, as shown in Fig.11. In the mutual information we can observe that a decoupling between the scales occurs at $k \approx 2 \times 10^{-2}$ which corresponds to a spatial scale of $\sim 10^2(m)$ (remember that if the mutual information is of the order of 0 then the joint pdf of the system can be decomposed into a product $\rho(u_{k<}, u_{k>}) = \rho(u_{k<})\rho(u_{k>})$).

Previously, the Shannon's entropy has been interpreted as system's predictability [**?**], in this sense we see that the largest scales are the least predictable. However, when

Preprints (www.preprints.org) | NOT PEER-REVIEWED | Posted: 18 November 2022 doi:10.20944/preprints202211.0347.v1

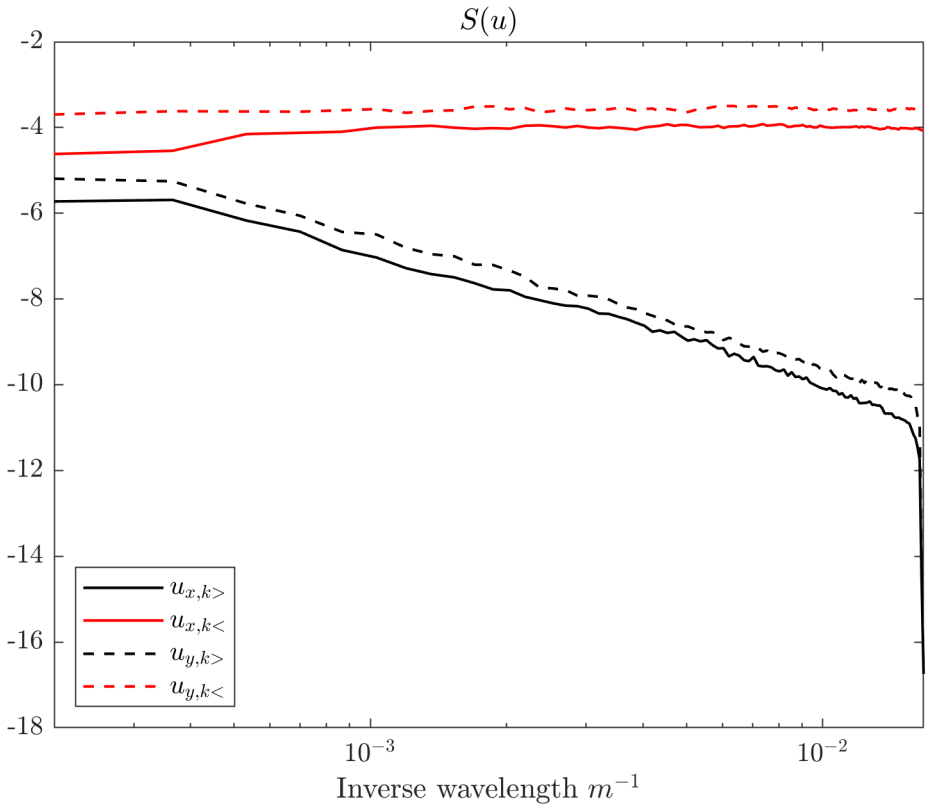

Figure 11. Entropy distribution

complementing this interpretation with mutual information, we see that on large scales it is also where more information is contained in the interactions, until the decoupling of the pdf occurs on small scales.

5. Summary and Conclusions

A modified state of the art Computational Fluid Dynamics code [21] is used as a framework to implement a highly resolved LES model of a mid-latitude upper ocean front. Through numerical simulations we investigate the spectral energy flux at the submesoscale/small-scale range in order to assess the inverse and forward kinetic energy fluxes at these scales and inquire into the processes which drive them in the absence of any atmospheric forcing. At the surface we find, a strong direct kinetic energy flux. In this upper ocean region the subgrid momentum diffusion is also intense. Computed deviation from the gradient wind balance shows that these processes are partially imbalanced, with some frontogenetic regions even exhibiting a mostly balanced dynamics.

In deeper waters calculations predict mostly an inverse kinetic energy flux. Deeper than 50 m depth we do not observe submesoscale conditions as $Ro < 0.4$ and frontogenesis is almost imperceptible, at 75 m depth there are only a few small regions with frontogenetic activity.

At the surface, the front shows significant coupling at scales larger than $\sim 10^3\ (m)$. This is manifested as a strong direct energy cascade and intense communication between scales. At scales smaller than $\sim 10^3\ (m)$ the results show near-zero energy flux associated with a weakly energetically coupled scales of motion, however, at the same scale range the estimator of mutual information flow still shows values that evidence a significant level of communication between them. This motivates to investigate the nature of the self-organized turbulent motion at this scale range with weak energetic coupling but where communication between scales is still significant and to inquire into the existence of synchronization or functional relationships between scales with emphasis on eventual

Preprints (www.preprints.org) | NOT PEER-REVIEWED | Posted: 18 November 2022 doi:10.20944/preprints202211.0347.v1

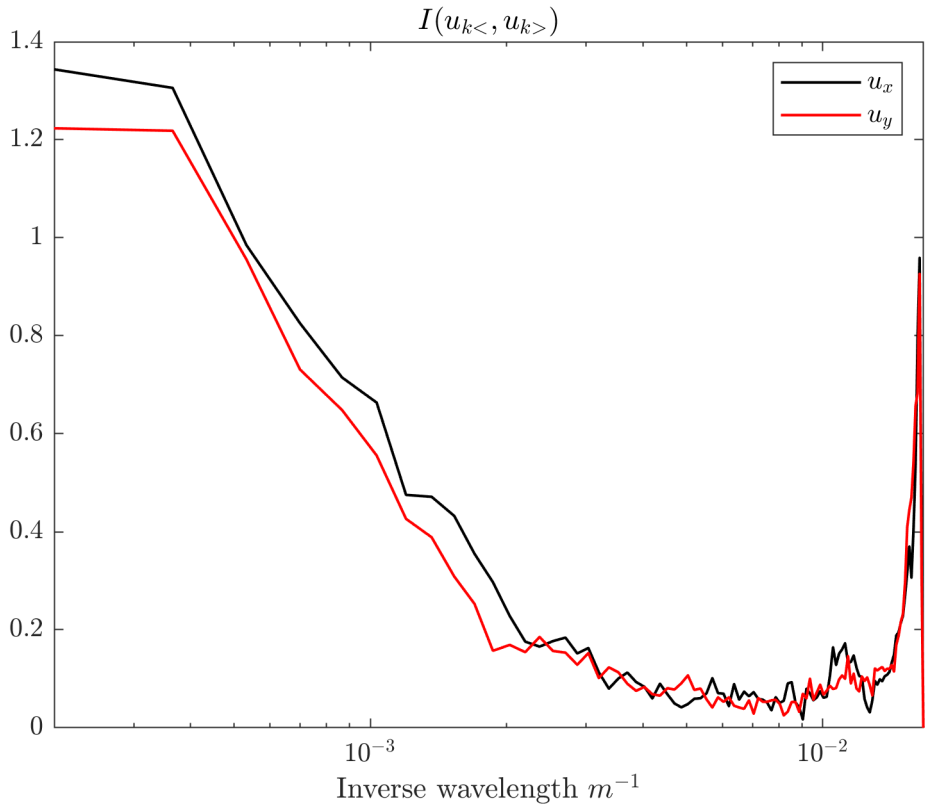

Figure 12. Mutual Communication between scales

underlying non-local processes. This would allow to create a more complex picture in the mechanics of turbulence as a property of self-organizing complex systems whose behavior would be characterized by processes involving transfer of energy and information.

Funding: This research received no external funding.

Institutional Review Board Statement: Not applicable.

Acknowledgments: This research was funded by the Interdisciplinary Center for Aquaculture Research (INCAR; FONDAP Project Number 15110027; CONICYT). The model simulations were run at the Laboratory of Computational Mechanics of the Department of Mechanical Engineering of the University of Concepción (Concepción, Chile).

Conflicts of Interest: The authors declare no conflict of interest.

Abbreviations

The following abbreviations are used in this manuscript:

LES	Large Eddy Simulation
CFD	Computational Fluid Dynamics
SIMPLE	Semi-Implicit Method for Pressure-Linked Equations
KSG	Kraskov-Stögbauer-Grassberger
KL	Kozachenko-Leonenko

References

1. Sullivan, P.P.; McWilliams, J.C. Frontogenesis and frontal arrest of a dense filament in the oceanic surface boundary layer. *J. Fluid Mech.* **2018**, *837*, 341–380.
2. Nikurashin, M.; Vallis, G.K.; Adcroft, A. Routes to energy dissipation for geostrophic flows in the Southern Ocean. *Nature Geoscience* **2012**, *6*, 48–51.

3. Shcherbina, A.Y.; D'Asaro, E.A.; Lee, C.M.; Klymak, J.M.; Molemaker, M.J.; McWilliams, J.C. Statistics of Vertical, Divergence, and Strain in a Developed Submesoscale Turbulence Field. *Geophysical research leters* **2013**, *40*, 4706–4711.
4. Capet, X.; McWilliams, J.C.; Molemaker, M.J.; Shchepetkin, a.F. Mesoscale to Submesoscale Transition in the California Current System. Part III: Energy Balance and Flux. *Journal of Physical Oceanography* **2008**, *38*, 2256–2269.
5. McWilliams, J.C. Fluid Dynamics at the Margin of Rotational Control. *Environmental Fluid Mechanics* **2008**, *8*, 441–449.
6. Thomas, L.N.; Tandon, A.; Mahadevan, A. Submesoscale Processes and Dynamics. *Ocean Modeling in an Eddy Regime* **2008**, pp. 17–38.
7. Mahadevan, a.; Tandon, a.; Ferrari, R. Rapid changes in Mixed Layer Stratification Driven by Submesoscale Instabilities and Winds. *Journal of Geophysical Research* **2010**, *115*, C03017.
8. Capet, X.; McWilliams, J.C.; Molemaker, M.J.; Shchepetkin, a.F. Mesoscale to Submesoscale Transition in the California Current System. Part II: Frontal Processes. *Journal of Physical Oceanography* **2008**, *38*, 44–64.
9. Marino, R.; Pouquet, A.; Rosenberg, D. Resolving the Paradox of Oceanic Large-Scale Balance and Small-Scale Mixing. *Physical Review Letters* **2015**, *114*, 1–5.
10. Müller, P.; McWilliams, J.; Molemaker, J. Routes to Dissipation in the Ocean: The 2D/3D Turbulence Conundrum. *Marine turbulence: theories, observations and models* **2005**, pp. 1–23.
11. Lévy, M.; Ferrari, R.; Franks, J.; Martin, A.P.; Riviere, P. Bringing Physics to Life at the Submesoscale. *Geophysical Research Letters* **2012**, *39*, 1–41.
12. Hoskins, B.J.; Bretherton, F. Amospheric Frontogenesis Models: Mathematical Formulation and Solution. *Jornal of atmospheric sciences* **1972**, *29*, 11–37.
13. Hoskins, B.J. The Mathematical Theory of Frontogenesis. *Annual Review of Fluid Mechanics* **1982**, *14*, 131–151.
14. Lee, C.; Rainville, L.; Harcourt, R.; Thomas, L. Enhanced Turbulence and Energy Dissipation at Ocean Fronts. *Science* **2011**, *332*, 318–322.
15. Nagai, T.; Tandon, A.; Yamazaki, H.; Doubell, M.J. Evidence of Enhanced Turbulent Dissipation in the Frontogenetic Kuroshio Front Thermocline. *Geophysical Research Letters* **2009**, *36*, 1–6.
16. Cerbus, R.; Goldburg, W. Information content of turbulence. *Physical Review E* **2013**, *88*, 053012.
17. Granero-Belinchón, C.; Roux, S.G.; Garnier, N.B. Kullback-Leibler divergence measure of intermittency: Application to turbulence. *Physical Review E* **2018**, *97*, 013107.
18. Granero-Belinchon, C.; Roux, S.G.; Garnier, N.B. Scaling of information in turbulence. *EPL (Europhysics Letters)* **2016**, *115*, 58003.
19. Lozano-Durán, A.; Arranz, G. Information-theoretic formulation of dynamical systems: causality, modeling, and control. *Physical Review Research* **2022**, *4*, 023195.
20. Wang, W.; Chu, X.; Lozano-Durán, A.; Helmig, R.; Weigand, B. Information transfer between turbulent boundary layers and porous media. *Journal of Fluid Mechanics* **2021**, *920*.
21. Cornejo, P.; Sepúlveda, H. Computational Fluid Dynamics Modelling of a Midlatitude Small scale Upper ocean front (accepted). *Jornal of Applied Fluid Mechanics* **2015**.
22. Smagorinsky, J. General Circulation Experiments with the Primitive Equations. I. The Basic Experiment. *Monthly weather review* **1963**, *91*, 99–164.
23. Scotti, A.; Meneveau, C.; Lilly, D.K. Generalized Smagorinsky Model for Anisotropic Grids. *Physics of Fluids A: Fluid Dynamics* **1993**, *5*, 2306–2308.
24. Stone, P. On the Geostrophic Baroclinic Stability. *Journal of Physical Oceanography* **1966**, *23*, 390–400.
25. Stone, P. A Simplified Radiative-dynamical Model for the Static Stability of Rotating Atmospheres. *J. Atmos. Sci.* **1972**, *29*, 405–418.
26. McWilliams, J.C. A Uniformly Valid Model Spanning the Regimes of Geostrophic and Isotropic, Stratified Turbulence: Balanced Turbulence. *Journal of the Atmospheric Sciences* **1985**, *42*, 1773–1774.
27. Skyllingstad, E.D.; Samelson, R.M. Baroclinic Frontal Instabilities and Turbulent Mixing in the Surface Boundary Layer. Part I: Unforced Simulations. *Journal of Physical Oceanography* **2012**, *42*, 1701–1716.
28. Kozachenko, L.F.; Leonenko, N.N. Sample estimate of the entropy of a random vector. *Problemy Peredachi Informatsii* **1987**, *23*, 9–16.
29. Kraskov, A.; Stögbauer, H.; Grassberger, P. Estimating mutual information. *Physical review E* **2004**, *69*, 066138.
30. Kraskov, A.; Stögbauer, H.; Grassberger, P. Estimating mutual information. *Physical review E* **2004**, *69*, 066138. Number: 6 Publisher: APS.
31. Charney, J.G. Geostrophic Turbulence. *Journal of the Atmospheric Sciences* **1971**, *28*, 1087–1095.
32. Blumen, W. Uniform Potential Vorticity Flow: Part I. Theory of Wave Interactions and Two-Dimensional Turbulence. *Journal of the Atmospheric Sciences* **1978**, *35*, 774–783.
33. Capet, X.; Klein, P.; B, L.H.; Lapeyre, G.; Mcwilliams, J.C. Surface Kinetic Energy Transfer in Surface Quasi-geostrophic Flows. *Journal of Fluid Mechanics* **2008**, *604*, 165–174.
34. Boyd, J.P. The Energy Spectrum of Fronts: Time Evolution of Shocks in Burgers' Equation. *Journal of the Atmospheric Sciences* **1992**, *49*, 128–139.
35. Higgins, C.; Parlange, M.B.; Meneveau, C. Energy issipation in Large-Eddy Simulation: Dependence on Flow Structure and Effects of Eigenvector Alignments. In *Atmospheric Turbulence and Mesoscale Meteorology*; 2004; pp. 51–70.